

Shell Structure and ρ -Tensor Correlations in Density-Dependent Relativistic Hartree-Fock theory

WenHui Long,^{1,2,*} Hiroyuki Sagawa,² Nguyen Van Giai,^{3,4} and Jie Meng¹

¹*School of Physics, Peking University, 100871 Beijing, China*

²*Center for Mathematical Sciences, University of Aizu,
Aizu-Wakamatsu, 965-8580 Fukushima, Japan*

³*Institut de Physique Nucléaire, CNRS-IN2P3, F-91406 Orsay Cedex, France*

⁴*Université Paris-Sud, F-91405 Orsay, France*

A new effective interaction PKA1 with ρ -tensor couplings for the density-dependent relativistic Hartree-Fock (DDRHF) theory is presented. It is obtained by fitting selected empirical ground state and shell structure properties. It provides satisfactory descriptions of nuclear matter and the ground state properties of finite nuclei at the same quantitative level as recent DDRHF and RMF models. Significant improvement on the single-particle spectra is also found due to the inclusion of ρ -tensor couplings. As a result, PKA1 cures a common disease of the existing DDRHF and RMF Lagrangians, namely the artificial shells at 58 and 92, and recovers the realistic sub-shell closure at 64. Moreover, the proper spin-orbit splittings and well-conserved pseudo-spin symmetry are obtained with the new effective interaction PKA1. Due to the extra binding introduced by the ρ -tensor correlations, the balance between the nuclear attractions and the repulsions is changed and this constitutes the physical reason for the improvement of the nuclear shell structure.

PACS numbers: 21.30.Fe, 21.60.Jz, 21.10.Dr, 24.10.Cn, 24.10.Jv

Keywords: Tensor force; Shell structure; RHF method; DDRHF theory

I. INTRODUCTION

Within the relativistic scheme, mean field theory has achieved great success in the description of finite nuclei and nuclear matter during the past years. One of the most outstanding models is the relativistic Hartree approach with the no-sea approximation, namely the relativistic mean field (RMF) theory [1, 2, 3]. The RMF theory provides appropriate quantitative descriptions for both stable and exotic nuclei with a limited number of free parameters, i.e., meson masses and meson-nucleon coupling constants [4, 5, 6, 7, 8, 9, 10, 11, 12]. Especially, the RMF model provides a natural mechanism for explaining the spin-orbit splittings in nuclear spectra with the covariant formulation of the strong scalar and vector fields. This feature becomes even more of central importance with the experimental

*Electronic address: whlong@pku.org.cn

observation that nuclei near drip lines undergo a modification of their shell structure, where the spin-orbit potential must play an essential role.

In the framework of the RMF approach, however, there exist two serious defects. One is the missing of one-pion exchange process. Namely, with the relativistic Hartree approach, the one-pion exchange has zero contribution in mediating nuclear interactions. Because of its small rest mass, one cannot simulate the one-pion exchange contributions with zero-range limit. It is expected that the one-pion exchange may have minor effects in the spin-saturated system, whereas in the unsaturated systems it plays an essential role in determining the isospin dependence of the shell evolutions [13]. Another problem is the tensor correlations, e.g., the ρ -tensor couplings. In the Hartree approximation, the contributions from the tensor couplings are practically negligible. In recent non-relativistic [14, 15] and relativistic studies [13], it is shown that the tensor forces have distinct effects on the shell evolution of nuclei [16]. In fact these two defects are mainly due to the absence of Fock terms which are dropped in RMF.

During the past decades, there have been several attempts to include the Fock terms in the relativistic description of nuclear systems [17, 18, 19, 20]. These relativistic Hartree-Fock (RHF) approaches could not provide satisfactory quantitative descriptions for the nuclear structure properties compared to the RMF approach. This is mainly due to the numerical complexity induced by the inclusion of Fock terms, which strongly increase the difficulties to find appropriate effective Lagrangians for the RHF approach. Recently a new RHF method, the density-dependent relativistic Hartree-Fock (DDRHF) theory [21] has brought a new insight to this problem. With the effective Lagrangians of Refs. [21, 22], the DDRHF theory can describe the ground state properties of many nuclear systems quantitatively on the same level as RMF. In addition, the investigations about the nuclear shell structure evolution within the DDRHF theory indicate that the one-pion exchange has a significant effect on the isospin dependence of the shell evolution [13].

However, some artificial shell structures, e.g., $Z = 58$ and $Z = 92$ appear in the calculations of RMF [23] as well as RHF. These spurious shells lead to the overbinding problem in these regions [24] and they also affect strongly the isospin dependence of the shell evolutions [13]. The relative positions of $1g_{7/2}$ and $2d_{5/2}$ states induce an artificial shell closure at $Z = 58$. The corresponding states for $Z = 92$ are $1h_{9/2}$ and $2f_{7/2}$. As a common feature, all these states are high- j states. Then, the single-particle energies of these states will be strongly affected by the tensor force [13], e.g., ρ -tensor couplings, which was not included in RMF or DDRHF before. In order to solve this artificial shell structure problem, we consider the ρ -tensor correlations in this work. In **Section II**, we introduce the ρ -tensor couplings in the DDRHF theory, where a new effective interaction PKA1 with the ρ -tensor coupling is presented. In **Section III**, the detailed investigation of the nuclear structure is performed with the newly obtained effective interaction PKA1. The conclusions are drawn in **Section IV**.

II. DDRHF THEORY WITH ρ -TENSOR COUPLING

The starting point of the DDRHF theory is the Lagrangian associated with nucleon (ψ), isoscalar σ - and ω -mesons, isovector ρ - and π -mesons, and photon (A) fields [21, 22]. In the isoscalar channels, the σ -scalar and ω -vector couplings provide the main part of the nuclear interactions, i.e., the short-range repulsive and mid-, long-range attractive interactions, respectively. One of the distinct differences of RHF from RMF is that all the mesons, including the isoscalar ones, have significant contributions to the isospin part of nuclear interactions. In Refs. [13, 21, 22, 25], the ρ -vector and π -pseudo-vector couplings were introduced in the calculations of DDRHF. The recent investigation about the role of one-pion exchange in DDRHF shows that the tensor type force has the strong effects on the nuclear structure [13]. In this study, we introduce the ρ -tensor correlations into the DDRHF theory in order to have a better understanding of the shell structure and cure the artificial shell structure problems of DDRHF and RMF [23].

A. General Formalism for ρ -Nucleon Couplings

In the DDRHF theory, the part of the Lagrangian containing the ρ -meson fields can be written as

$$\mathcal{L}_\rho = -\frac{1}{4}\vec{R}_{\mu\nu} \cdot \vec{R}^{\mu\nu} + \frac{1}{2}m_\rho^2\vec{\rho}_\mu \cdot \vec{\rho}^\mu - g_\rho\bar{\psi}\gamma_\mu\vec{\tau}\psi + \frac{f_\rho}{2M}\bar{\psi}\sigma_{\mu\nu}\partial^\nu\vec{\rho}^\mu \cdot \vec{\tau}\psi, \quad (1)$$

where $\vec{R}_{\mu\nu} = \partial_\mu\vec{\rho}_\nu - \partial_\nu\vec{\rho}_\mu$, and m_ρ denotes the rest mass of the isovector-vector ρ -meson ($\vec{\rho}_\nu$), and g_ρ and f_ρ are the vector and tensor coupling strengths, respectively.

From the Lagrangian (1), one can obtain the equation of motion for the ρ -meson field as,

$$[\square + m_\rho^2] \vec{\rho}_\nu = g_\rho\bar{\psi}\gamma_\nu\vec{\tau}\psi + \partial^\mu \frac{f_\rho}{2M}\bar{\psi}\sigma_{\nu\mu}\vec{\tau}\psi, \quad (2)$$

which leads to the general form of ρ -meson field,

$$\vec{\rho}_\nu(x) = \int d^4y \left[g_\rho\bar{\psi}\gamma_\nu\vec{\tau}\psi - \frac{f_\rho}{2M}\bar{\psi}\sigma_{\nu\mu}\vec{\tau}\psi\partial^\mu \right]_y D_\rho(x, y) \quad (3)$$

where D_ρ is the ρ -meson propagator.

With the Legendre transformation (ϕ_i is the field variables of the Lagrangian \mathcal{L}),

$$\mathcal{H}_\rho = \frac{\partial\mathcal{L}_\rho}{\partial\dot{\phi}_i}\dot{\phi}_i - \mathcal{L}_\rho, \quad (4)$$

the Hamiltonian of the ρ -meson field can be obtained as,

$$H_\rho = \frac{1}{2} \int d^3x \left[g_\rho\bar{\psi}\gamma^\nu\vec{\tau}\psi - \frac{f_\rho}{2M}\bar{\psi}\sigma^{\nu l}\vec{\tau}\psi\partial_l \right]_x \cdot \vec{\rho}_\nu(x). \quad (5)$$

In the above expression, we neglect the time component of the four-momentum carried by the mesons, which amounts to ignoring the retardation effects.

With the quantization of the nucleon field ψ [18] and the general form of the ρ -meson field (3), the Hamiltonian H_ρ can be written as,

$$H_\rho^{(i)} = \frac{1}{2} \sum_{\alpha\beta\gamma\delta} c_\alpha^\dagger c_\beta^\dagger c_\gamma c_\delta \langle \tau_\alpha | \vec{\tau}_1 | \tau_\delta \rangle \cdot \langle \tau_\beta | \vec{\tau}_2 | \tau_\gamma \rangle \times \int d\mathbf{r}_1 d\mathbf{r}_2 \bar{f}_\alpha(\mathbf{r}_1) \bar{f}_\beta(\mathbf{r}_2) [\Gamma_\rho^i(1,2)v(m_\rho; 1, 2)] f_\gamma(\mathbf{r}_2) f_\delta(\mathbf{r}_1) , \quad (6)$$

where the Yukawa factor $v(m_\rho; 1, 2)$ is

$$v(m_\rho; 1, 2) = \frac{1}{4\pi} \frac{e^{-m_\rho |\mathbf{r}_1 - \mathbf{r}_2|}}{|\mathbf{r}_1 - \mathbf{r}_2|} . \quad (7)$$

The inclusion of ρ -tensor correlations leads to three types of interactions in Eq. (6): the Vector (V), Tensor (T) and Vector-Tensor (VT) couplings. The corresponding vertex matrix $\Gamma_\rho^i(1,2)$ in Eq. (6) can be expressed as,

$$\Gamma_\rho^V(1, 2) = g_\rho(1)\gamma_\mu g_\rho(2)\gamma^\mu(2), \quad (8a)$$

$$\Gamma_\rho^T(1, 2) = \frac{1}{4M^2} f_\rho(1)\sigma_{\nu k}(1)f_\rho(2)\sigma^{\nu l}(2)\partial^k(1)\partial_l(2), \quad (8b)$$

$$\Gamma_\rho^{VT}(1, 2) = \frac{1}{2M} \left[f_\rho(1)\sigma^{k\nu}(1)g_\rho(2)\gamma_\nu(2)\partial_k(1) + g_\rho(1)\gamma_\nu f_\rho(2)\sigma^{k\nu}(2)\partial_k(2) \right]. \quad (8c)$$

Detailed expressions about the energy functional of ρ -meson field can be found in Refs. [18, 21].

In DDRHF, the meson-nucleon coupling constants are treated as a function of baryonic density ρ_b . Here we take the same functional form for the density-dependence of the isoscalar mesons (g_σ and g_ω) as in Ref. [21]:

$$g_i(\rho_b) = g_i(\rho_0)f_i(\xi), \quad \text{for } i = \sigma, \omega, \quad (9)$$

where

$$f_i(\xi) = a_i \frac{1 + b_i(\xi + d_i)^2}{1 + c_i(\xi + d_i)^2} \quad (10)$$

with $\xi = \rho_b/\rho_0$, and ρ_0 denotes the saturation density of nuclear matter. For the isovector mesons as well as the newly introduced ρ -tensor coupling f_ρ , the exponential density-dependence is adopted as,

$$g_i = g_i(0)e^{-a_i \xi} . \quad (11)$$

In the above expression, $g_i(0)$ corresponds to the free coupling constants g_ρ , f_ρ , and f_π , and a_i are the corresponding parameters a_ρ , a_T and a_π , respectively.

For the open shell nuclei, the pairing correlations are treated by the BCS method and the pairing matrix elements are calculated with a zero-range, density-dependent interaction [26]

$$V(r_1, r_2) = V_0 \delta(r_1 - r_2) \left[1 - \frac{\rho_b(r)}{\rho_0} \right] , \quad (12)$$

where $V_0 = -900 \text{ MeV}\cdot\text{fm}^3$. The active pairing space is limited to the single-particle states below the single-particle energy $+15 \text{ MeV}$.

In this work, the corrections from the center-of-mass motion are treated in the same way as in Refs. [11, 22]. For the numerical calculations, a box boundary condition at 20fm is introduced for the unbound states as well as the bound ones and we check that the overall results are not affected by the choice of the box size. For the radial step, one may choose smaller one about 0.05 fm in the light nuclei whereas 0.1 fm is precise enough for the heavy nuclei.

B. New Effective Interaction

In the previous DDRHF parametrizations (PKO1, PKO2 and PKO3) [13, 21, 22], we selected 12 nuclei as the reference ones, i.e., ^{16}O , ^{40}Ca , ^{48}Ca , ^{56}Ni , ^{68}Ni , ^{90}Zr , ^{116}Sn , ^{132}Sn , ^{182}Pb , ^{194}Pb , ^{208}Pb and ^{214}Pb . In the present case for PKA1, we aim to cure the artificial shell structure problem at $Z = 58$ and 92 . To solve this problem and recover the sub-shell closure at $Z = 64$, two more nuclei $^{140}_{58}\text{Ce}_{82}$ and $^{146}_{64}\text{Gd}_{82}$ are added as the reference nuclei and ^{56}Ni is replaced by its neighboring one ^{58}Ni . The parameter fitting procedure is similar to that in Refs. [11, 22]. Besides the bulk properties (ρ_0 , K and J) of nuclear matter and the binding energies of the reference nuclei, we include the spin-orbit splittings of neutron and proton $1p$ states of ^{16}O , and the shell gaps at $Z = 58$ ($^{140}_{58}\text{Ce}_{82}$) and $Z = 64$ ($^{146}_{64}\text{Gd}_{82}$) as the new criteria. By minimizing the χ^2 error as in Ref. [22], we obtain the new effective interaction PKA1 with the ρ -tensor coupling for the DDRHF theory (see **Table I**). In this parametrization, we have 12 free parameters, 6 in the isoscalar channels as well as 6 in the isovector channels. We slightly change the coupling strength for π -meson (f_π and a_π) in PKA1 from the effective interaction PKO1 [21], which is the starting Lagrangian in the fitting process.

TABLE I: Parameters of new effective interaction PKA1. The quantity κ is $\kappa = f_\rho/g_\rho$, the ratio of the vector and tensor couplings of ρ -meson. The masses (in MeV) of nucleon, ω -, ρ - and π -mesons are taken as $M = 938.9$, $m_\omega = 783.0$, $m_\rho = 769.0$ and $m_\pi = 138.0$, respectively.

m_σ	488.227904	a_σ	1.103589	a_ω	1.126166
g_σ	8.372672	b_σ	16.490109	b_ω	0.108010
g_ω	11.270457	c_σ	18.278714	c_ω	0.141251
ρ_0	0.159996	d_σ	0.135041	d_ω	1.536183
g_ρ	3.649857	κ	3.199491	f_π	1.030722
a_ρ	0.544017	a_T	0.820583	a_π	1.200000

In **Fig. 1**, the density-dependent couplings g_σ , g_ω (left panels) and g_ρ , f_ρ , and f_π (right panels) of the effective interaction PKA1 are shown as functions of the baryonic density ρ_b , in comparison with PKO1 (DDRHF) [21] and DD-ME2 (RMF) [27]. As seen from **Fig. 1**, the density-dependence

of isoscalar couplings, especially for g_σ , is weak for PKA1 compared to PKO1 and DD-ME2. For the isovector channels, g_ρ , f_ρ and f_π show strong density-dependence in PKA1 whereas the density-dependence of g_ρ of PKO1 is weak. For the one-pion exchange, PKA1 and PKO1 have nearly the same coupling strength for f_π . PKA1 and PKO1 have smaller coupling strength in magnitude for both the isoscalar and isovector channels compared to DD-ME2. This is mainly due to the effects of the Fock terms. One can also find that the inclusion of ρ -tensor coupling leads to smaller g_σ and larger g_ω in PKA1 than those in PKO1. This indicates that the ρ -tensor correlations contribute to make the nuclear interactions attractive.

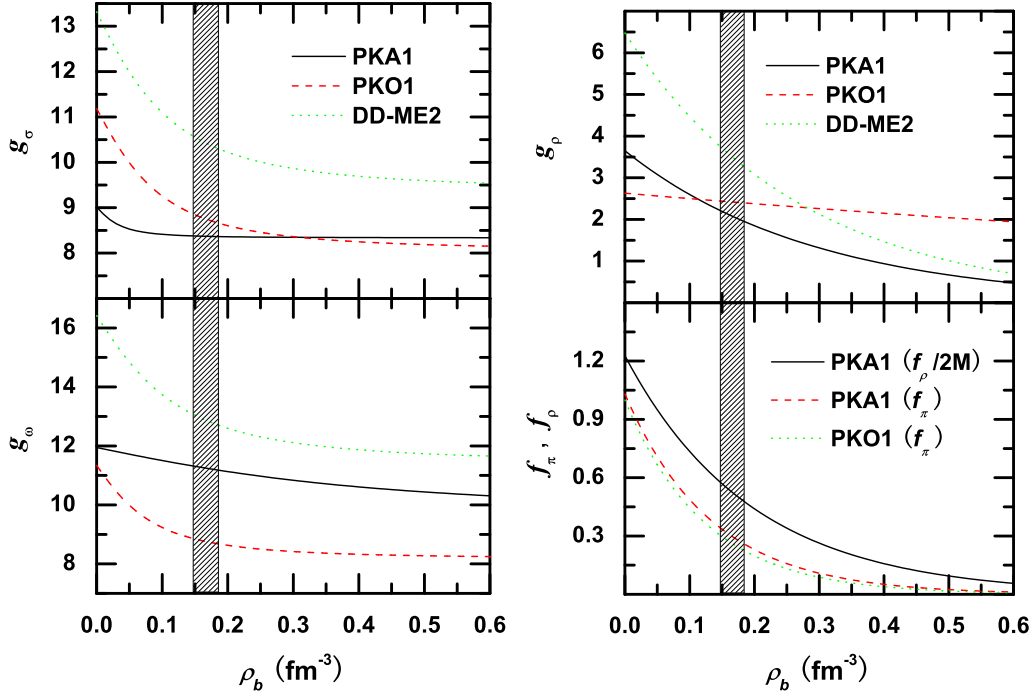


FIG. 1: (color online) The density-dependent meson-nucleon couplings in the isoscalar (left panel: g_σ and g_ω) and isovector (right panel: g_ρ , f_ρ and f_π) channels as functions of density for the new DDRHF effective interaction PKA1, in comparison with PKO1 in DDRHF and DD-ME2 in RMF. The shadowed area denotes the empirical saturation density region.

We calculate the bulk properties of nuclear matter with the effective interaction PKA1 as shown in **Table II**, where the results calculated by DDRHF with PKO1 and RMF with DD-ME2 are also listed for comparison. Compared to PKO1 and DD-ME2, PKA1 gives a larger saturation density ρ_0 , which is close to the common value in non-relativistic HF calculations. Although PKA1 gives a smaller compression modulus K and a larger symmetry energy J , the values are still acceptable. Among these three effective interactions, PKO1 has the largest effective masses (the relativistic one M_R^* and the non-relativistic one M_{NR}^*) [21] whereas DD-ME2 gives smallest ones. Comparing the values of M_{NR}^* and M_S^* , one can find a significant difference between DDRHF and RMF, the DDRHF models giving a larger difference between these two masses. Actually this difference is of special importance

in describing nuclear structure since the effective mass M_{NR}^* is related to the level density whereas the scalar mass M_S^* is related to the spin-orbit splitting. In the following, one may find the corresponding effects due to this difference.

TABLE II: The saturation density ρ_0 (fm^{-3}), the binding energy E_B (MeV), the compression modulus K (MeV), the symmetry energy J (MeV), the effective masses M_{R}^* and M_{NR}^* [21], and the scalar mass M_S^* for the symmetric nuclear matter. The results are calculated with PKA1 and PKO1 in DDRHF, and with DD-ME2 in RMF.

	ρ_0	E_B	K	J	M_{R}^*	M_{NR}^*	M_S^*
PKA1	0.160	-15.83	229.96	36.02	0.663	0.681	0.547
PKO1	0.152	-16.00	250.24	34.37	0.727	0.746	0.590
DD-ME2	0.152	-16.14	250.97	32.30	0.635	0.652	0.572

As we have mentioned before, 14 reference nuclei are adopted in the parametrization of PKA1. The binding energies and charge radii of these nuclei calculated with PKA1 are shown in **Table III** in comparison with the calculations of PKO1 [21], DD-ME2 [27], and the experimental data [28, 29, 30]. Other reference nuclei than the present 14 ones used in the parametrizations PKO1 and DD-ME2 are listed in the lower panel of **Table III**. In this table, the root mean square deviations (rmsd) Δ and relative rmsd δ are defined as

$$\Delta^2 \equiv \frac{1}{N} \sum_{i=1}^N \left(y_i^{\text{Exp.}} - y_i^{\text{Cal.}} \right)^2, \quad (13a)$$

$$\delta^2 \equiv \frac{1}{N} \sum_{i=1}^N \left(1 - y_i^{\text{Cal.}} / y_i^{\text{Exp.}} \right)^2. \quad (13b)$$

From the values of Δ and δ in **Table III**, we can see that PKA1 provides an appropriate description for both binding energies and charge radii of these reference nuclei. For the binding energies, PKA1 gives the best agreement with the data. For the charge radii, PKA1 gives quantitatively comparable description to PKO1 and DD-ME2. Since the reference nuclei cover from light (^{16}O) to heavy (^{214}Pb , ^{210}Po) ones, one may expect that DDRHF with the tensor interaction PKA1 can provide a proper description of the nuclei in the whole nuclear chart.

The charge densities calculated with PKA1 and PKO1 for the nuclei ^{16}O , ^{40}Ca , ^{48}Ca , ^{90}Zr and ^{208}Pb are presented in **Fig. 2**. The experimental data [29] are also shown for comparison. One can see that DDRHF with PKA1 provides a fairly good agreement with the data in heavy systems, e.g., ^{208}Pb and ^{90}Zr . For ^{40}Ca and ^{48}Ca PKA1 also shows comparable quality to PKO1 whereas it presents less good agreement for ^{16}O . In **Table III**, one can also find better agreement in the heavy nuclei than in the light ones for the charge radii calculated with PKA1.

TABLE III: Binding energies and charge radii for the reference nuclei. The results are calculated by DDRHF with the new effective interaction PKA1 and with PKO1 [21], and by RMF with DD-ME2 [27]. The upper panel gives the reference nuclei of PKA1 and the other reference nuclei of PKO1 and DD-ME2 are listed in the lower panel. Experimental data are taken from Refs. [28, 29, 30].

Nuclide	E_b (MeV)				r_{ch} (fm)			
	Exp.	PKA1	PKO1	DD-ME2	Exp.	PKA1	PKO1	DD-ME2
^{16}O	-127.6193	-126.9913	-128.3250	-127.9640	2.7370	2.7996	2.6757	2.6703
^{40}Ca	-342.0520	-341.7177	-343.2747	-343.0046	3.4852	3.5251	3.4423	3.4417
^{48}Ca	-415.9904	-416.3697	-417.3713	-414.9174	3.4837	3.4916	3.4501	3.4568
^{58}Ni	-506.4584	-505.9705	-502.9424	-501.0959	3.7827	3.7006	3.7195	3.7387
^{68}Ni	-590.4077	-590.1520	-591.4448	-591.6165		3.8766	3.8480	3.8651
^{90}Zr	-783.8919	-784.3525	-784.6039	-782.4711	4.2720	4.2794	4.2501	4.2574
^{116}Sn	-988.6835	-986.9107	-987.7642	-986.8494	4.6257	4.6056	4.5924	4.6061
^{132}Sn	-1102.8508	-1103.2468	-1103.5838	-1102.9335		4.6985	4.6964	4.7047
^{140}Ce	-1172.6915	-1170.0999	-1177.5650	-1175.3038	4.8774	4.8836	4.8672	4.8690
^{146}Gd	-1204.4353	-1202.0964	-1205.0765	-1203.2093	4.9838	4.9889	4.9669	4.9771
^{182}Pb	-1411.6534	-1409.7315	-1412.7060	-1411.0088		5.3831	5.3708	5.3819
^{194}Pb	-1525.8907	-1521.9706	-1523.8836	-1522.1179	5.4446	5.4488	5.4334	5.4431
^{208}Pb	-1636.4301	-1636.9604	-1636.9108	-1638.0676	5.5046	5.5103	5.5051	5.5092
^{214}Pb	-1663.2906	-1661.3564	-1662.4803	-1659.5703	5.5622	5.5600	5.5619	5.5605
Δ		1.6847	1.8787	2.3495		0.0342	0.0341	0.0298
δ		0.19%	0.30%	0.34%		1.03%	1.01%	0.94%
^{56}Ni	-483.9917	-486.2191	-483.0607	-481.1788		3.6662	3.6899	3.7114
^{72}Ni	-613.1694	-613.8442	-615.1913	-613.1482		3.9029	3.8795	3.8964
^{124}Sn	-1049.9627	-1049.9471	-1050.1779	-1049.0708	4.6739	4.6649	4.6477	4.6602
^{204}Pb	-1607.5059	-1605.8114	-1606.7831	-1606.4818	5.4861	5.4936	5.4857	5.4908
^{210}Po	-1645.2125	-1644.7950	-1646.4921	-1646.9803		5.5482	5.5393	5.5425
Δ		1.5927	1.7256	2.1784		0.0317	0.0322	0.0277
δ		0.20%	0.27%	0.32%		0.95%	0.94%	0.87%

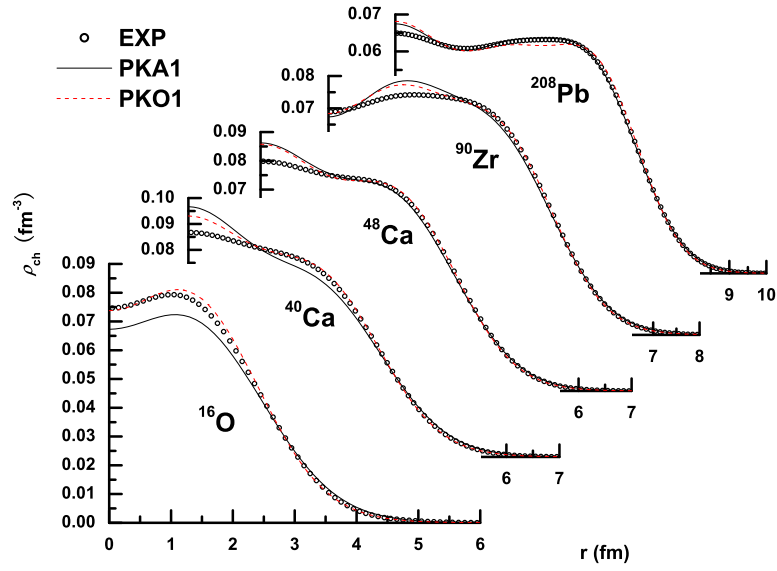


FIG. 2: (color online) Charge distributions of ^{16}O , ^{40}Ca , ^{48}Ca , ^{90}Zr and ^{208}Pb . The results are calculated with PKA1 and PKO1. Experimental data are taken from Ref. [29].

III. NUCLEAR STRUCTURE PROPERTIES WITH TENSOR CORRELATIONS

A. Single-particle Spectra

In **Section II**, we showed that the effective interaction PKA1 can describe quantitatively well the bulk properties of nuclear matter and the ground state properties of finite nuclei. In this section, we study the shell structure of the Hartree-Fock single-particle energies for several reference nuclei by using PKA1. For comparison, we also show the results of the reference nuclei calculated with three other interactions: PKO1 (DDRHF without ρ -tensor couplings), PK1 [11] (RMF with non-linear self-couplings of mesons), DD-ME2 (RMF with density-dependent meson-nucleon couplings).

In **Fig. 3** and **Fig. 4** are shown the neutron (left panel) and proton (right panel) single-particle levels in ^{140}Ce and ^{146}Gd , respectively. For these two $N = 82$ isotones, their proton numbers correspond to the artificial shell closure $Z = 58$ occurring in RMF and the sub-shell closure $Z = 64$ observed in experiments, respectively. In the results calculated with PKO1, PK1, and DD-ME2, one can find large shell gaps at $Z = 58$ or $N = 58$ in both nuclei. These gaps are even comparable to the well established shell gaps $Z = 50$ and $N = 82$. In contrast, PKA1 brings much smaller shell gaps at $N = 58$ and $Z = 58$ in the single-particle levels of ^{140}Ce In ^{146}Gd , the artificial shell structures $Z = 58$ and $N = 58$ completely disappear and the sub-shell closures $Z = 64$ and $N = 64$ are well reproduced by PKA1.

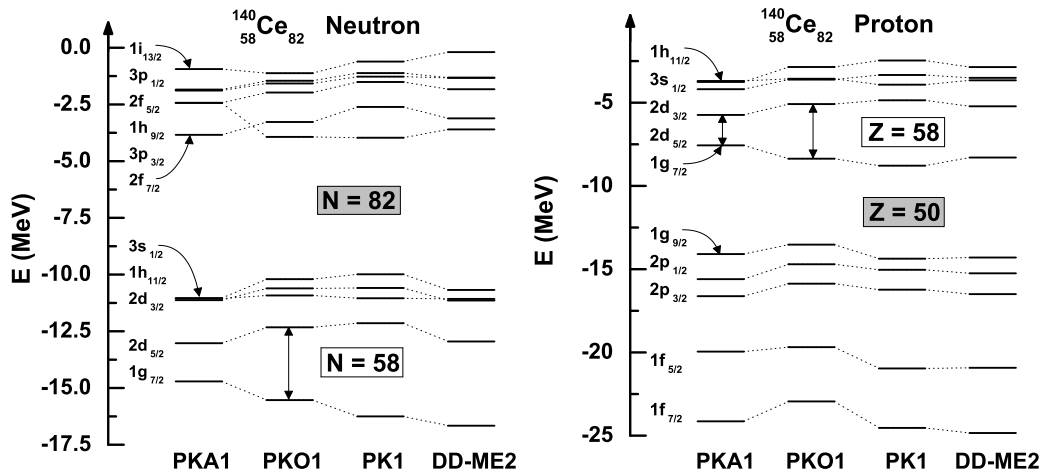


FIG. 3: Single-particle energies of ^{140}Ce . The results are calculated by DDRHF with PKA1 and PKO1, and RMF with PK1 and DD-ME2.

Besides ^{140}Ce and ^{146}Gd , we also calculated another $N = 82$ isotone, the doubly magic nucleus ^{132}Sn . In **Fig. 5** are shown the neutron (left panel) and proton (right panel) single-particle levels calculated with PKA1, PKO1, PK1, and DD-ME2. The experimental data from Ref. [31] are also shown for comparison. In this figure, one can also find the spurious shell structures Z or $N = 58$ appearing in the results of PKO1, PK1, and DD-ME2. Compared to these three results, PKA1 shows

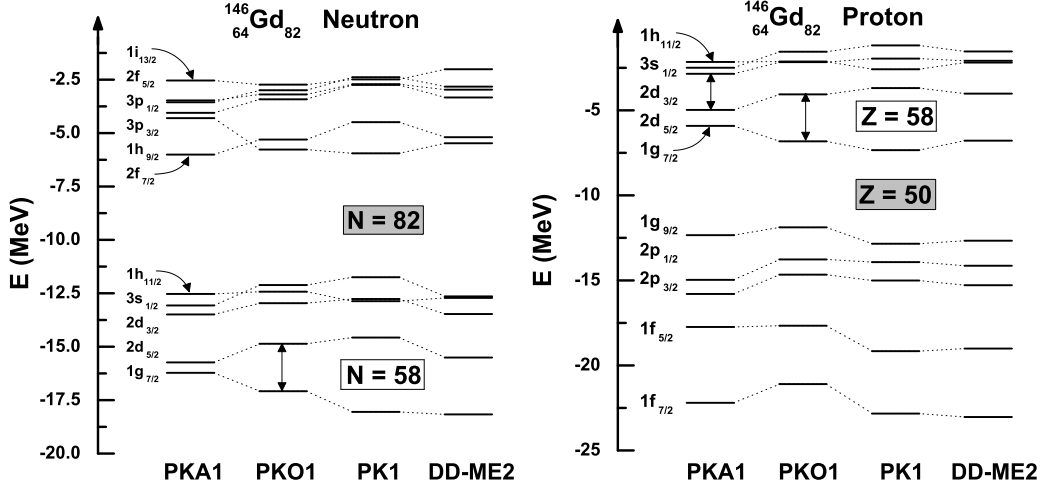


FIG. 4: Single-particle energies of ^{146}Gd . The results are calculated by DDRHF with PKA1 and PKO1, and RMF with PK1 and DD-ME2.

distinct improvement on this problem. Namely, the spurious shell gaps do not appear any more and fairly good agreement with the data is obtained with PKA1.

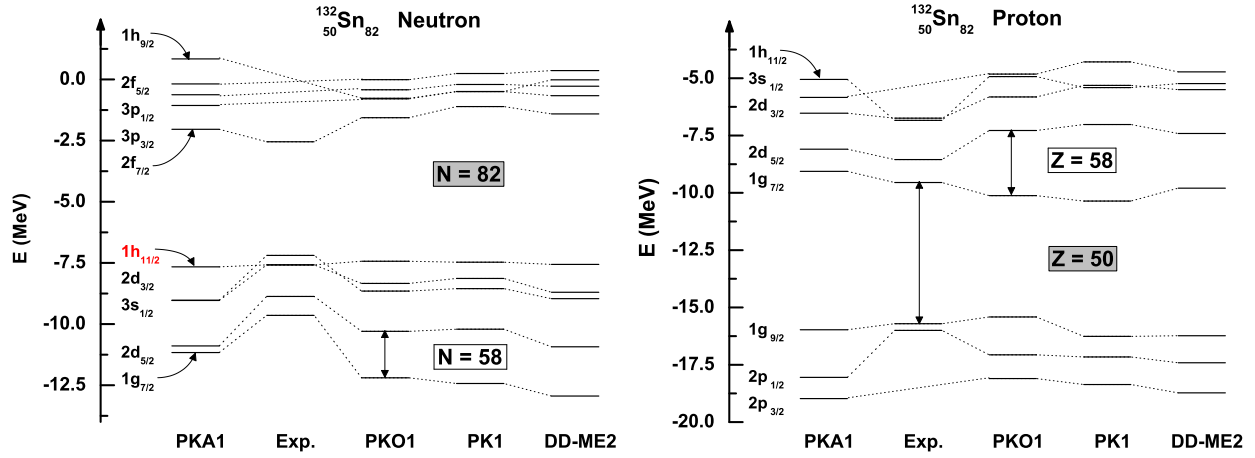


FIG. 5: Single-particle energies of ^{132}Sn . The results are calculated by DDRHF with PKA1 and PKO1, and RMF with PK1 and DD-ME2. Experimental data are taken from Ref. [31].

It is well known that the two-nucleon separation energy is an important criteria to identify the nuclear shell structure. In **Fig. 6**, the two-proton separation energy S_{2p} calculated with PKA1, PKO1 and DD-ME2 are shown as a function of proton number Z for the $N = 82$ isotones, and the experimental data [28] are also shown for comparison. A sudden change of the slope is found in the results of PKO1 and DD-ME2 at $Z = 58$. This is a clear sign of the existence of spurious shell structure at $Z = 58$ in the calculations of the existing DDRHF and RMF Lagrangians. In contrast, the two-proton separation energy calculated by PKA1 decreases smoothly as a function of Z and agrees well with the experimental data. **Fig. 6** shows that the spurious shell structure $Z = 58$ is successfully

eliminated by the new DDRHF effective interaction PKA1.

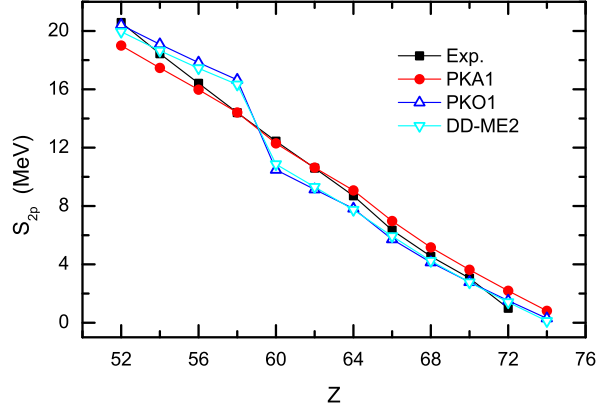


FIG. 6: (color online) Two-proton separation energies of the $N = 82$ isotones. The results are calculated by DDRHF with PKA1 and PKO1, and RMF with DD-ME2. The experimental data are taken from Ref. [28].

Besides N (or Z) = 58, the nucleon number 92 is another spurious shell structure in the calculations of RMF [23]. In **Fig. 7**, it is clearly shown in both neutron and proton single-particle spectra that N (or Z) = 92 becomes a spurious shell structure in the results of PKO1, PK1, and DD-ME2. With the inclusion of the ρ -tensor correlations, the artificial shell closures at $N = 92$ and $Z = 92$ disappear in both neutron and proton spectra in the results of PKA1. In addition, PKA1 also shows another improvement in the order of single-particle levels, e.g., for the neutron states $2g_{9/2}$ and $1i_{11/2}$ in ^{208}Pb . Namely, DDRHF with PKA1 provides the same ordering with the data while the other three cases fail to predict the correct ordering.

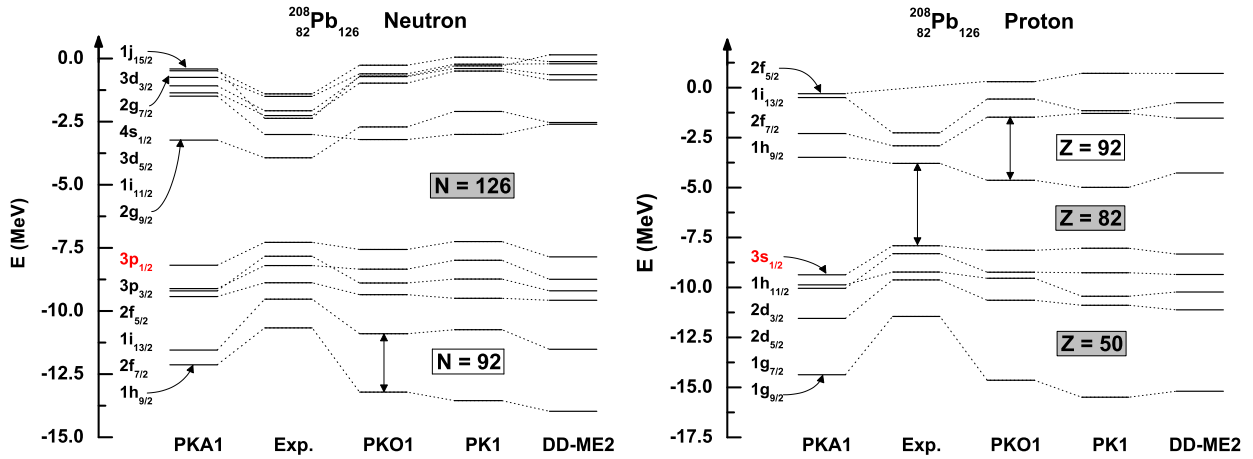


FIG. 7: Single-particle energies of ^{208}Pb . The results are calculated by DDRHF with PKA1 and PKO1, and RMF with PK1 and DD-ME2. The experimental data are taken from Ref. [31].

B. Spin-orbit Splittings and ρ -Tensor Correlations

From the discussions on the single-particle spectra of several reference nuclei, one can find significant improvements with the inclusion of ρ -tensor correlations in DDRHF calculations. The spin-orbit splitting is also very essential to test the validity of the model. In **Table IV**, we give the spin-orbit splittings in several magic nuclei obtained by using PKA1, PKO1, and DD-ME2. The experimental data are also tabulated for comparison. As seen from this table, PKA1 provides comparable quantitative results of the spin-orbit splittings to PKO1 and DD-ME2. Among the results calculated with PKA1, there are some systematic over estimations of the spin-orbit splittings of some states, e.g., $\nu 1f$ in ^{48}Ca and ^{56}Ni , $\nu 1g$ in ^{90}Zr , $\pi 1g$ in ^{132}Sn , and $\nu 1i$, $\pi 1h$ in ^{208}Pb , which account for the corresponding shell closures. For these spin partner states, one of the partners is not occupied and one may expect sizable corrections from particle-vibration coupling. In the present calculations, the particle-vibration coupling is not included yet, and its effects generally tend to shift the occupied and unoccupied states to the Fermi surface. Therefore, the systematic over estimation of the spin-orbit splittings may leave some space for this effect.

TABLE IV: The spin-orbit splittings (in MeV) of neutron (ν) and proton (π) states for the magic nuclei calculated with PKA1, PKO1, and DD-ME2. The experimental data are taken from Ref. [31].

Nucleus	State	Exp.	PKA1	PKO1	DD-ME2	Nucleus	State	Exp.	PKA1	PKO1	DD-ME2
^{16}O	$\nu 1p$	6.18	6.055	6.426	6.545	^{56}Ni	$\nu 1f$	6.82	10.027	7.363	8.361
	$\pi 1p$	6.32	5.973	6.356	6.472		$\nu 2p$	1.11	0.899	0.977	1.383
^{40}Ca	$\nu 1d$	6.75	7.386	6.742	6.760	^{90}Zr	$\nu 2p$	0.37	1.702	1.598	1.686
	$\nu 2p$	2.00	2.527	1.846	1.694		$\nu 2d$	2.42	2.457	2.049	2.097
	$\pi 1d$	5.94	7.215	6.629	6.696		$\nu 1g$	7.07	8.608	7.155	7.609
^{48}Ca	$\nu 1d$	5.30	6.817	5.414	6.172	^{208}Pb	$\pi 2p$	1.51	1.489	1.430	1.619
	$\nu 1f$	8.01	8.512	7.345	7.737		$\nu 2f$	2.14	2.342	2.009	2.317
	$\nu 2p$	1.67	1.647	1.347	1.462		$\nu 2g$	2.38	2.482	2.103	2.322
	$\pi 1d$	5.01	6.833	5.590	6.406		$\nu 1i$	5.81	7.936	6.143	6.970
	$\pi 2p$	2.14	1.634	1.322	1.539		$\nu 3p$	0.90	0.925	0.782	0.889
^{132}Sn	$\nu 2d$	1.66	1.866	1.645	1.969	$\nu 3d$	0.89	0.875	0.710	0.726	
	$\pi 1g$	5.33	6.909	5.291	6.438	$\pi 2d$	1.53	1.506	1.404	1.769	
	$\pi 2d$	1.75	1.569	1.463	1.912	$\pi 1h$	5.03	6.380	4.901	5.955	

From the Dirac equation, one can express the single-particle energy for a state a as

$$E_a = E_{k,a} + E_{\sigma,a} + E_{\omega,a} + E_{\rho,a} + E_{\pi,a} + E_{A,a} + E_{R,a} , \quad (14)$$

where $E_{k,a}$ denotes the kinetic contribution, and $E_{i,a}$ ($i = \sigma, \omega, \rho, \pi, A$) represent the contributions from the mesons and photon coupling channels including the direct and exchange parts, and $E_{R,a}$

accounts for the rearrangement terms. From Eq. (14), one can also obtain the contributions to the spin-orbit splittings from different channels.

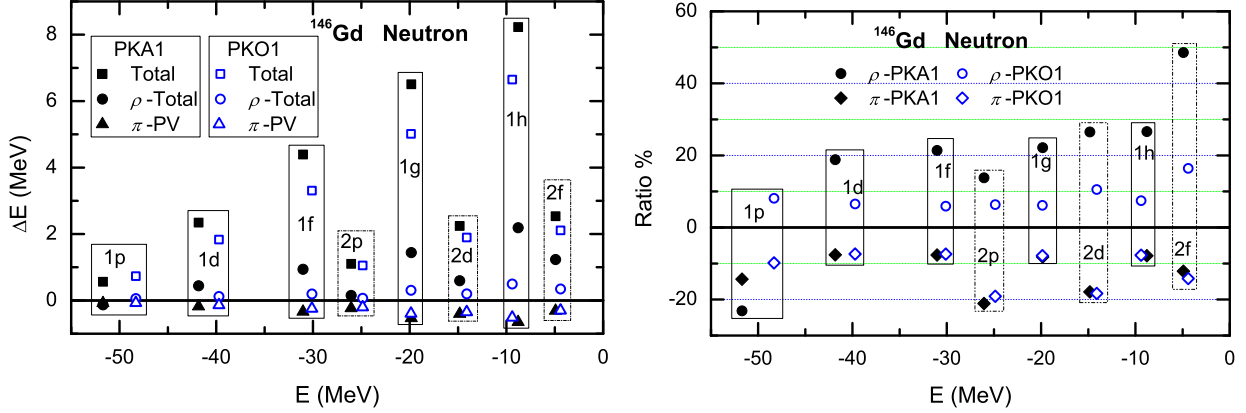


FIG. 8: Contributions from ρ - and π -mesons to the spin-orbit splittings for the neutron orbits in ^{146}Gd calculated by DDRHF with PKA1 and PKO1. The left panel shows the total values of the spin-orbit splittings and the contributions from the ρ - and π -mesons, and the right panel shows the ratios of the ρ - and π -mesons contributions to the spin-orbit splittings.

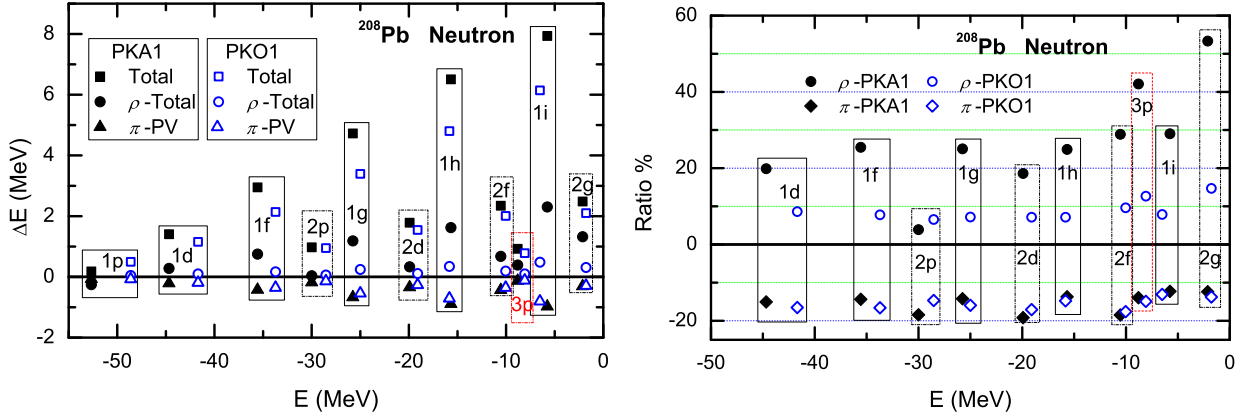


FIG. 9: Similar as Fig. 8, but for ^{208}Pb .

In order to understand the improvement on the shell structure brought by the ρ -tensor couplings, we compare the contributions of the ρ - and π -mesons to the spin-orbit splittings between two DDRHF effective interactions PKA1 and PKO1. In Fig. 8 and Fig. 9, are shown the contributions to the spin-orbit splittings from ρ - and π -mesons, respectively for the ^{146}Gd and ^{208}Pb neutron orbits. From these two figures, one can find that the π pseudo-vector (PV) coupling gives almost same contributions to the spin-orbit splittings in PKA1 (filled up-triangles) and PKO1 (open up-triangles). This can be well explained by the equivalent π -coupling strength in these two effective interactions. For the contributions from ρ -meson, PKA1 and PKO1 have distinct difference. Due to the tensor interactions, the ρ -meson coupling in PKA1 (filled circles) shows substantially larger effects than that of PKO1 (open circles). It is seen that the average contributions from the ρ -meson couplings in PKA1 are

about 20% of the total ones. For the states near the Fermi surface or some high- j orbits, the ρ -meson contribution grows up to 30% and even higher. On the other hand, the ρ -meson coupling of PKO1 gives about 10% in most cases. The π -meson gives opposite contributions to the ρ -meson for the spin-orbit splittings except the $1p$ states and the magnitude is about (10~20)% of the spin-orbit splitting. Because of the tensor effects in π -PV couplings, some systematic enhancements are also observed in high- j states like $1g$ and $1h$ states in ^{146}Gd , and $1h$ and $1i$ in ^{208}Pb . As was noticed in the comparison between PKA1 and PKO1, the ρ -tensor couplings have significant effects on the spin-orbit splittings, especially for high- j orbits, and affect much the shell structures. This is the main reason why the improvement of the shell structure is obtained with the ρ -tensor correlations.

C. Spurious Shell closures and Pseudo-spin symmetry

As we mentioned before, the spurious shell closures at 58 and 92 are related with the pairs of high- j states $\{2d_{5/2}, 1g_{7/2}\}$ and $\{2f_{7/2}, 1h_{9/2}\}$, respectively. These pairs are the pseudo-spin partners, $1\tilde{f}$ and $1\tilde{g}$ states, respectively. The spurious shell closure problem is then related to the conservation of pseudo-spin symmetry (PSS) [25, 32, 33, 34, 35, 36, 37], i.e., the existing artificial shell structures in RMF break largely PSS. As seen from the results of PKA1 (see **Fig. 4** and **Fig. 7**), PSS is successfully recovered for the $1\tilde{f}$ states in ^{146}Gd and $1\tilde{g}$ states in ^{208}Pb . In order to understand the improvement due to the ρ -tensor correlations, we studied the contributions from different terms in Eq. (14) to the pseudo-spin orbital splittings. In **Table V** and **Table VI** are shown the results calculated by DDRHF with PKA1 (upper panels) and PKO1 (lower panels) respectively for ^{146}Gd and ^{208}Pb neutron orbits. One can find in these results that PKA1 conserves pseudo-spin symmetry better than PKO1 for the states near the Fermi levels, e.g., $\nu 1\tilde{f}$ and $\nu 2\tilde{p}$ states in ^{146}Gd , $\nu 1\tilde{g}$ and $\nu 2\tilde{d}$ states in ^{208}Pb .

For the pseudo-spin orbital splittings, PKA1 and PKO1 provide similar contributions in magnitude to the kinetic part (ΔE_k), the rearrangement term (ΔE_R), and the π -coupling (ΔE_π) except for a few cases. For the contributions from σ -, ω -mesons ($\Delta E_{\sigma+\omega}$) and ρ -meson (ΔE_ρ) couplings, there exist a distinct difference between PKA1 and PKO1, especially for the states near the Fermi surfaces. From these two tables one can see that the ρ -meson couplings in PKA1 give larger contributions to the pseudo-spin orbital splittings than those in PKO1 and the ρ -tensor couplings increase the splittings. For the states near the Fermi surface, PKA1 provides negative values of $\Delta E_{\sigma+\omega}$, which cancel largely with ΔE_k and ΔE_ρ . In the PKO1 results, the $\Delta E_{\sigma+\omega}$ is always positive and only the rearrangement term ΔE_R partially cancels the contributions from the other channels.

To understand the differences between the results of PKA1 and PKO1, we study the contributions from different terms to the average binding energy \bar{E} of the spin partner states j_1 and j_2 , i.e., $\bar{E} = [E_1(2j_1 + 1) + E_2(2j_2 + 1)] / (2j_1 + 2j_2 + 2)$. In the left panel of **Fig. 10**, the average binding energies

TABLE V: The contributions (in MeV) from different terms in Eq. (14) to the pseudo-spin orbital splittings ΔE for neutron (ν) orbits in ^{146}Gd , calculated by DDRHF with PKA1 (upper panel) and PKO1 (lower panel). The average binding energy \bar{E} for the pseudo-spin partner states j_1 and j_2 is $[E_1(2j_1 + 1) + E_2(2j_2 + 1)] / (2j_1 + 2j_2 + 2)$.

^{146}Gd	State	\bar{E}	ΔE	ΔE_ρ	ΔE_π	ΔE_R	ΔE_k	$\Delta E_{\sigma+\omega}$	ΔE_σ	ΔE_ω
PKA1	$\nu 1\tilde{p}$	-39.44	2.935	0.277	0.039	0.080	1.900	0.639	11.391	-10.751
	$\nu 1\tilde{d}$	-27.68	2.097	0.476	0.225	-0.439	2.592	-0.756	14.847	-15.603
	$\nu 1\tilde{f}$	-16.01	0.489	1.107	0.525	-1.187	2.546	-2.502	18.145	-20.647
	$\nu 2\tilde{p}$	-13.35	0.422	0.602	0.344	-0.456	0.854	-0.920	7.499	-8.419
PKO1	$\nu 1\tilde{p}$	-37.63	2.985	0.429	0.041	-0.370	1.521	1.364	8.502	-7.138
	$\nu 1\tilde{d}$	-27.02	3.013	0.493	0.180	-0.814	2.131	1.023	12.372	-11.349
	$\nu 1\tilde{f}$	-16.13	2.224	0.662	0.404	-1.360	1.945	0.573	18.306	-17.733
	$\nu 2\tilde{p}$	-12.68	0.851	0.387	0.284	-0.524	0.188	0.516	9.315	-8.799

TABLE VI: Same as **Table V**, for ^{208}Pb neutron orbits.

^{208}Pb	State	\bar{E}	ΔE	ΔE_ρ	ΔE_π	ΔE_R	ΔE_k	$\Delta E_{\sigma+\omega}$	ΔE_σ	ΔE_ω
PKA1	$\nu 1\tilde{p}$	-42.74	3.292	0.342	0.083	-0.006	1.655	1.218	7.555	-6.337
	$\nu 1\tilde{d}$	-32.46	3.560	0.329	0.218	-0.111	2.393	0.730	14.699	-13.969
	$\nu 1\tilde{f}$	-22.06	2.502	0.608	0.455	-0.563	2.738	-0.735	20.507	-21.242
	$\nu 1\tilde{g}$	-11.87	0.584	1.181	0.757	-1.251	2.431	-2.535	23.240	-25.776
	$\nu 2\tilde{p}$	-18.76	0.259	0.265	0.233	-0.399	1.177	-1.017	3.704	-4.721
	$\nu 2\tilde{d}$	-9.17	0.092	0.777	0.459	-0.695	0.773	-1.222	5.289	-6.510
PKO1	$\nu 1\tilde{p}$	-40.04	2.851	0.238	0.100	-0.349	1.370	1.492	4.663	-3.172
	$\nu 1\tilde{d}$	-31.04	3.644	0.421	0.207	-0.712	2.009	1.720	10.406	-8.686
	$\nu 1\tilde{f}$	-21.66	3.397	0.549	0.380	-1.125	2.212	1.381	16.130	-14.749
	$\nu 1\tilde{g}$	-12.18	2.314	0.619	0.604	-1.530	1.731	0.890	21.939	-21.048
	$\nu 2\tilde{p}$	-17.95	0.678	0.117	0.181	-0.348	0.624	0.105	4.354	-4.250
	$\nu 2\tilde{d}$	-8.67	0.547	0.183	0.371	-0.566	0.124	0.434	8.938	-8.503

\bar{E} and the sum of the kinetic part (\bar{E}_k), the σ - and ω -couplings (\bar{E}_σ and \bar{E}_ω) are shown as a function of angular momentum l for the neutron orbits of ^{208}Pb . The right panel shows the rearrangement term (\bar{E}_R), and the sum of the ρ - and π -coupling terms (\bar{E}_ρ and \bar{E}_π). The results are calculated with PKA1 (filled symbols) and PKO1 (open symbols). In the left panel, it is found that PKA1 provides stronger l -dependence than PKO1 for the average binding energy \bar{E} . In the results of PKO1, the main contribution to \bar{E} is given by the sum $\bar{E}_k + \bar{E}_\sigma + \bar{E}_\omega$, whereas in the results of PKA1, \bar{E}_R and $\bar{E}_\rho + \bar{E}_\pi$ also provide significant contributions to \bar{E} . This is due to the fact that \bar{E}_R and $\bar{E}_\rho + \bar{E}_\pi$ cancel each other in the results of PKO1 as shown in the right panel. On the other hand, PKA1 gives

weaker rearrangement term \bar{E}_R , and much stronger ρ -couplings than PKO1. Thus, the inclusion of ρ -tensor couplings give significant contributions to the nuclear attraction, which strongly affects on the coupling strength in other channels, e.g., PKA1 has a stronger ω -coupling than PKO1 as shown in **Fig. 1**.

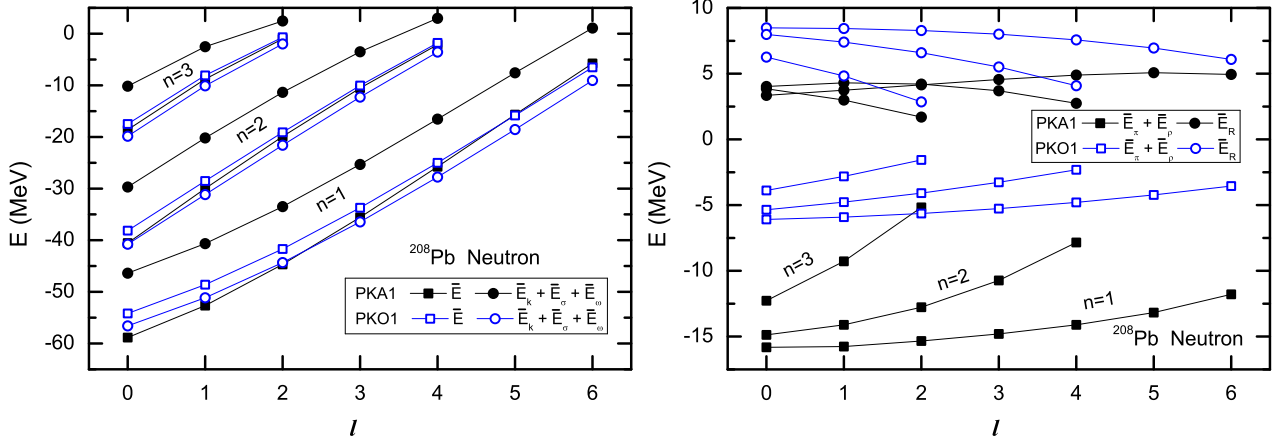


FIG. 10: The average binding energy $\bar{E} = [E_1(2j_1 + 1) + E_2(2j_2 + 1)] / (2j_1 + 2j_2 + 2)$ of the ^{208}Pb neutron orbits as a function of the angular momentum l calculated by DDRHF with PKA1 (filled symbols) and PKO1 (open symbols). Left panel gives the sum contributions from the kinetic part (\bar{E}_k), the σ - and ω -couplings (\bar{E}_σ and \bar{E}_ω) to the average binding energy and the total ones, and right panel shows the contributions from the rearrangement term (\bar{E}_R), the ρ -, and π -couplings (\bar{E}_ρ and \bar{E}_π).

In **Fig. 11** are shown the values of \bar{E}_σ and \bar{E}_ω calculated with PKA1 (filled symbols) and PKO1 (open symbols) as a function of angular momentum l . One can see that PKA1 leads to a stronger l -dependence of \bar{E}_ω than PKO1, and to a similar (slightly stronger) l -dependence of \bar{E}_σ for the states near the Fermi surface. It should be noticed that the pseudo-spin partner states have different angular momenta l . The stronger l -dependence of \bar{E}_ω given by PKA1 leads to larger negative contributions to the pseudo-spin orbital splittings as shown in the last column of **Table V** and **Table VI**. These results finally induce negative values for $\Delta E_{\sigma+\omega}$ so that PSS can be well conserved in the results of PKA1. As a relativistic symmetry, the conservation of the PSS is mainly determined by the balance of the nuclear attractions and repulsions [38], which is also well demonstrated by **Table V** and **Table VI**. Compared to the PKO1 results, this balance is much changed by PKA1 due to the extra binding induced by the ρ -tensor couplings, which indicates the physical reason for the improvement of the nuclear shell structure.

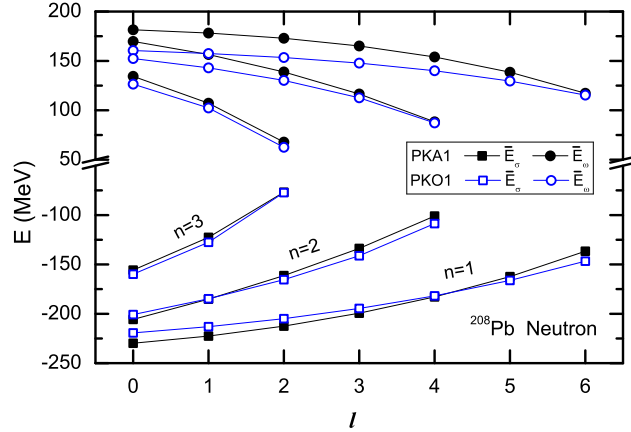


FIG. 11: Contributions from the σ - and ω -couplings (\bar{E}_σ and \bar{E}_ω) to the average binding energy $\bar{E} = [E_1(2j_1 + 1) + E_2(2j_2 + 1)] / (2j_1 + 2j_2 + 2)$ of the ^{208}Pb neutron orbits as a function of the angular momentum l calculated with PKA1 (filled symbols) and PKO1 (open symbols).

IV. CONCLUSIONS

In this work, we have introduced the ρ -tensor correlations in the density-dependent relativistic Hartree-Fock (DDRHF) theory. By fitting the empirical properties of ground state and the shell structure, we propose a new DDRHF effective interaction with ρ -tensor couplings, PKA1. With the newly obtained effective interaction PKA1, DDRHF provides satisfactory descriptions of the bulk properties of nuclear matter and the ground state properties of finite nuclei, at the same quantitative level as the established DDRHF and RMF models.

Moreover, the inclusion of ρ -tensor correlations brings a significant improvement on the descriptions of nuclear shell structures compared to the existing DDRHF and RMF Lagrangians. Particularly, we have studied the single-particle spectra of nuclei ^{140}Ce , ^{146}Gd , ^{132}Sn and ^{208}Pb with PKA1 and compared to previous DDRHF and RMF approaches. It has been found that the previous DDRHF and RMF calculations give the spurious shell closures 58 and 92, whereas the realistic sub-shell closure 64 cannot be well reproduced. The effective interaction PKA1 cures these common diseases, eliminating the spurious shell structure and recovering the sub-shell closure 64. In addition, the inclusion of tensor correlations improves the descriptions of the ordering of the single-particle levels, e.g., the neutron states $2g_{9/2}$ and $1i_{11/2}$ in ^{208}Pb , which are important states for nuclear structure problems.

The spin-orbit splittings and the pseudo-spin orbital splittings of the magic nuclei are also studied by using PKA1, and the PKO1 version which has no ρ -tensor coupling. It is shown that the ρ -tensor correlations have substantial effects on enlarging both splittings, especially for the high- j states. Even though, PKA1 still provides an appropriate quantitative agreement with the experimental data on the spin-orbit splittings for the magic nuclei at the same level as the modern DDRHF and RMF Lagrangians. It is shown that the artificial shell structure problem is intimately related to the con-

servation of the pseudo-spin symmetry, which is determined by the balance of the nuclear attractions from σ -meson and ρ -tensor couplings and the repulsion from ω -meson coupling. It is found that a better conserved pseudo-spin symmetry is obtained with PKA1, in which the ρ -tensor correlations contribute significantly to the nuclear attraction. Due to the extra binding introduced by the ρ -tensor correlations, the balance of attraction and repulsion is changed by the parametrization PKA1, and this constitutes the physical reason for the improvement of the nuclear shell structure.

-
- [1] L. D. Miller and A. E. S. Green, *Phys. Rev.* **C 5**, 241 (1972).
 - [2] J. Walecka, *Ann. Phys. (N.Y.)* **83**, 491 (1974).
 - [3] B. Serot and J. D. Walecka, *Adv. Nucl. Phys.* **16**, 1 (1986).
 - [4] P.-G. Reinhard, *Reports on Progress in Physics* **52**, 439 (1989).
 - [5] P. Ring, *Prog. Part. Nucl. Phys.* **37**, 193 (1996).
 - [6] G. A. Lalazissis, J. König, and P. Ring, *Phys. Rev.* **C 55**, 540 (1997).
 - [7] B. D. Serot and J. D. Walecka, *Int. J. Mod. Phys.* **E 6**, 515 (1997).
 - [8] S. Typel and H. H. Wolter, *Nucl. Phys.* **A 656**, 331 (1999).
 - [9] T. Nikšić, D. Vretenar, P. Finelli, and P. Ring, *Phys. Rev.* **C 66**, 024306 (2002).
 - [10] M. Bender, P.-H. Heenen, and P.-G. Reinhard, *Revs. Mod. Phys.* **75**, 121 (2003).
 - [11] W. H. Long, J. Meng, N. V. Giai, and S.-G. Zhou, *Phys. Rev.* **C69**, 034319 (2004).
 - [12] J. Meng, H. Toki, S. G. Zhou, S. Q. Zhang, W. H. Long, and L. S. Geng, *Prog. Part. Nucl. Phys.* **57**, 470 (2006).
 - [13] W. H. Long, H. Sagawa, JieMeng, and N. V. Giai (2007), arXiv: nucl-th/0609076.
 - [14] T. Otsuka, T. Suzuki, R. Fujimoto, H. Grawe, and Y. Akaishi, *Phys. Rev. Lett.* **95**, 232502 (2005).
 - [15] G. Colò, H. Sagawa, S. Fracasso, and P. Bortignon, *Phys. Lett.* **B** (2007, in press).
 - [16] J. P. Schiffer, S. J. Freeman, J. A. Caggiano, C. Deibel, A. Heinz, C.-L. Jiang, R. Lewis, A. Parikh, P. D. Parker, K. E. Rehm, et al., *Phys. Rev. Lett.* **92**, 162501 (2004).
 - [17] A. Bouyssy, S. Marcos, J. F. Mathiot, and N. V. Giai, *Phys. Rev. Lett.* **55**, 1731 (1985).
 - [18] A. Bouyssy, J. F. Mathiot, N. V. Giai, and S. Marcos, *Phys. Rev.* **C 36**, 380 (1987).
 - [19] P. Bernardos, V. N. Fomenko, N. V. Giai, M. L. Quelle, S. Marcos, R. Niembro, and L. N. Savushkin, *Phys. Rev.* **C 48**, 2665 (1993).
 - [20] S. Marcos, L. N. Savushkin, V. N. Fomenko, M. López-Quelle, and R. Niembro, *J. Phys. G: Nucl. Part. Phys.* **30**, 703 (2004).
 - [21] W. H. Long, N. V. Giai, and J. Meng, *Phys. Lett.* **B 640**, 150 (2006).
 - [22] W. H. Long, N. V. Giai, and J. Meng, in preparation (2007), W. H. Long, Ph. D. Thesis and to be published.
 - [23] L. S. Geng, J. Meng, H. Toki, W.-H. Long, and G. Shen, *Chin. Phys. Lett.* **23**, 1139 (2006).
 - [24] L. S. Geng, H. Toki, and J. Meng, *Prog. Theo. Phys.* **113**, 785 (2005).
 - [25] W. H. Long, H. Sagawa, JieMeng, and N. V. Giai, *Phys. Lett.* **B 639**, 242 (2006).

- [26] J. Dobaczewski, W. Nazarewicz, T. R. Werner, J. F. Berger, C. R. Chinn, and J. Dechargé, *Phys. Rev. C* **53**, 2809 (1996).
- [27] G. A. Lalazissis, T. Nikšić, D. Vretenar, and P. Ring, *Phys. Rev. C* **71**, 024312 (2005).
- [28] G. Audi, A. H. Wapstra, and C. Thibault, *Nucl. Phys. A* **729**, 337 (2003).
- [29] H. de Vries, C. de Jager, and C. de Vries, *At. Data Nucl. Data Tables* **36**, 495 (1987).
- [30] E. G. Nadjakov and K. P. Marinova, *At. Data Nucl. Data Tables* **56**, 133 (1994).
- [31] A.-M. Oros, Ph. D. thesis, University of Köln (1996).
- [32] A. Arima, M. Harvery, and K. Shimizu, *Phys. Lett. B* **30**, 517 (1969).
- [33] K. Hecht and A. Adler, *Nucl. Phys. A* **137**, 129 (1969).
- [34] J. Meng, K. Sugawara-Tanabe, S. Yamaji, P. Ring, and A. Arima, *Phys. Rev. C* **58**, R628 (1998).
- [35] J. Meng, K. Sugawara-Tanabe, S. Yamaji, and A. Arima, *Phys. Rev. C* **59**, 154 (1999).
- [36] T. S. Chen, H. F. Lü, J. M. J, S. Q. Zhang, and S. G. Zhou, *Chin. Phys. Lett.* **20**, 358 (2003).
- [37] J. N. Ginocchio, *Phys. Rep.* **414**, 165 (2005).
- [38] J. Ginocchio, *Phys. Rev. Lett.* **78**, 436 (1997).